Innovative Mechanism Design for Data Mining and Enhanced Gear Misalignment Detection via Vibration Analysis

Amirhossein Amirnia, Somaye Mohammadi, Mehdi Behzad*

Condition Monitoring Center, Mechanical Engineering Department, Sharif University of Technology, Tehran, Iran

* Corresponding Author: somaye.mohammadi@sharif.edu

Accepted Manuscript

Abstract

With the rapid and ongoing advancement of industry and considering the crucial role of gearboxes in various machines and industrial systems, the monitoring and maintenance of these systems are of great importance. One of the most common faults in industrial gearboxes is misalignment between meshing gears. The presence of misalignment creates favorable conditions for the development of gear and bearing defects. Due to the widespread use of helical gears in most industrial gearboxes, a more in-depth investigation of their behavior under misalignment conditions is necessary. In this study, to better replicate real-world and industrial scenarios, experiments were conducted on an industrial gearbox operating under gear misalignment. A specialized mechanism was designed and fabricated to impose controlled misalignment. After collecting data and extracting vibration signals, nine features were calculated and analyzed. The results show that among these features, Energy Ratio and Kurtosis exhibited the highest percentage variations compared to the aligned condition. Additionally, detailed analysis reveals that these features showed more significant increases in the horizontal direction and at measurement points closer to the meshing location of the misaligned gears, compared to the aligned state.

Keywords

Condition monitoring, Fault diagnosis, Gear misalignment, Vibration analysis, Time synchronous averaging, Feature extraction

1. Introduction

Gearboxes play a vital role in various industries, including aerospace, energy systems, marine applications, and the automotive sector, serving as essential components that transmit the required power and torque to machinery. However, defects such as tooth wear, tooth cracks, tooth breakage, misalignment between engaged gears, bearing faults, and other related failures can lead to unexpected breakdowns, production downtime, increased maintenance costs, and even safety hazards. Among these defects, the occurrence of misalignment between gears is significant, as it alters the stress distribution on the tooth surface and creates stress concentration zones. Gear misalignment can also trigger secondary failures, including wear, pitting, tip breakage, and bearing defects. Therefore, early detection of gear misalignment and timely corrective actions are critical to preventing subsequent failures and ensuring reliable gearbox operation.

In this context, researchers have reported various models, experimental studies, and analytical investigations. In 2016, Hi *et al.* proposed a novel approach for analyzing vibration signals of a planetary gearbox in a wind turbine under both healthy and faulty conditions, with a specific focus on main shaft misalignment. Their innovative method relied on a discrete spectrum correction technique [1]. In 2019, Muhammad Ali Khan *et al.* investigated the variations in energy levels and statistical parameters, such as kurtosis and skewness, of vibration and acoustic signals for radial, axial, and combined misalignments. Their experiments were conducted on a single-stage gearbox with a pair of spur gears, using a laboratory setup to simulate different types of misalignments [2]. In 2020, Kane *et al.* investigated the capabilities of vibration-based and acoustic-based methods, as well as the psychoacoustic features of acoustic signals, in classifying and correlating gearbox defects. Simulated faults included tooth root cracks, tooth breakage, profile errors, and gear misalignment. The experiments were carried out on a single-stage gearbox with a pair of spur gears [3]. In the same year, Casu *et al.* examined the characteristics of acoustic signals obtained from a gearbox with shaft misalignment. The test rig was a two-stage, three-parallel-shaft helical gear system. Their findings highlighted that sensor placement plays a critical role in the quality and reliability of the acquired signals [4].

In 2022, Yang *et al.* presented a novel model incorporating gear misalignment and its influence on gear meshing stiffness. Their simulations were performed on spur gears [5]. In parallel, Vishnu *et al.* investigated the effectiveness of machine learning techniques for gearbox fault diagnosis, with a focus on vertical misalignment and tooth breakage. They applied a Long Short-Term Memory (LSTM) recurrent neural network model. They also demonstrated that time-domain vibration data yielded higher accuracy compared to frequency-domain data in both training and testing. They reported that this is due to information loss during frequency transformation. [6]. In 2023, Hu *et al.* developed a nonlinear dynamic model considering shaft misalignment for a pair of spur gears to investigate vibration responses. Their proposed model was validated using both simulations and available experimental results in the literature [7]. Similarly, Zou *et al.* proposed a dynamic model incorporating nonlinear Hertzian contact to examine the effects of angular misalignment on contact surfaces and gear meshing. Their model was validated through

Accepted Manuscript

experiments on a two-stage spur gear test rig [8]. Most recently, in 2024, Zhao *et al.* introduced a model of gear–bearing systems with shaft misalignment to extract dynamic response features of the system [9].

In recent years, various models, algorithms, and effective methods have been proposed for detecting gear misalignment. However, several key gaps need to be addressed when analyzing and detecting misalignment between gears. Most of the studies have been conducted on gearboxes equipped with spur gears. Since helical gears are widely used in most industrial gearboxes, conducting investigations on such gears becomes a priority. Moreover, in many previous studies, the employed gearboxes were specifically designed and constructed for laboratory experiments. As a result, research on an industrial gearbox can provide more realistic insights and enhance the validity of the findings. For example, most studies have investigated gear misalignment in the absence of lubrication. Considering the damping effect of vibrations in the presence of lubrication, examining this flaw with lubrication between the gears is of significant importance. Moreover, most setups investigated in the literature operate at high rotational speeds, highlighting the need for further studies on low-speed gearboxes under gear misalignment conditions.

The primary objective of this study is to address the limitations mentioned above in previous studies. Accordingly, this study aims to deliberately induce misalignment in an industrial helical gearbox equipped with an oil splash lubrication system, thereby considering the oiling process between gears. Furthermore, to account for the effects of low operating speed under misalignment conditions, the fault was introduced on the output shaft of the experimental setup, which operates at a maximum speed of 8.5 revolutions per minute. Labelled datasets, which are essential for developing intelligent models in future studies, will be generated during the process. Afterwards, the data will be processed using the Time Synchronous Averaging (TSA) technique. The goal is to identify reliable features that can be used for misalignment detection between helical gears in a condition that is as close to the real one as possible. For this purpose, a three-stage helical reduction gearbox is employed. To introduce misalignment, a dedicated mechanism has been designed and fabricated. This mechanism operates by modifying the bearings of the shaft and utilizing a two-piece eccentric end cover to impose a controlled deviation in the relative engagement of the gear teeth. Such a mechanism enables the generation of misalignment in different planes between the meshing gears.

In this section, the problem of gearbox misalignment is outlined, the related literature is reviewed, and the main gaps and objectives of this study are defined. The structure of the remainder of the paper is as follows. Section 2 describes the experimental test rig and the industrial gearbox setup. Section 3 presents the simulations and stress analysis between two misaligned gears. Section 4 outlines the signal processing and feature extraction method, while Section 5 details the design of the experiment and data acquisition. Section 6 discusses the results and their implications. Finally, Section 7 concludes the study with key findings and future perspectives.

Accepted Manuscript

2. Experimental test rig

This section introduces the industrial gearbox test rig developed for this research. The overall gearbox configuration, its main specifications, and photographs of the assembled system are presented to provide context. Furthermore, the procedure for creating controlled misalignment between the gears is described in detail in subsection 2.2. These descriptions serve as the basis for subsequent experimental and analytical investigations.

2.1. Industrial gearbox setup

In this study, an industrial gearbox, specifically a three-stage reduction gearbox with low RPM (Revolutions per Minute) output, has been employed. The gearbox is equipped with helical gears and utilizes a crown wheel at the input stage. Both the driving system and the loading mechanism of the gearbox are belt–pulley–based. The specifications of the electromotor and the gear pairs are presented in Table 1. In addition, photographs of the gears and the assembled test setup in the laboratory are shown in Figures 1a and 1 b.

Table 1. Technical specifications of the industrial gearbox test rig

Electromotor power	2 hp (1.5 kW)
Input nominal speed	1500 RPM (25 Hz)
Gear ratio	164.94
Teeth number	8/50, 13/83, 15,62

At the initial stage, considering the industrial application of the gearbox and the necessity of performing experiments solely under misalignment conditions, the gearbox setup and housing are thoroughly examined. Accordingly, a blue check test has been performed to observe the gear meshing pattern. This test, which is commonly applied during the installation of industrial gearboxes, is a method for inspecting the contact pattern of gear teeth. In this procedure, a thin layer of Prussian Blue dye is applied to the tooth surface, and by rotating the gear pair, the transferred pattern reveals the actual load distribution, thereby enabling the identification of misalignment, machining errors, and the accuracy of tooth engagement.

After conducting this test, it was observed that in the third stage, at the meshing location between the output shaft and the second idler shaft gears, the contact pattern is not uniform. Therefore, the concentricity of the DE and NDE housings of the gearbox has been examined in the machine workshop, and it was found that the housings of the output shaft exhibited a total misalignment of approximately 0.8 mm, which is likely due to prolonged and occasionally abnormal loading applied to the shaft. Therefore, the most critical defect identified in this setup

Accepted Manuscript

was the misalignment of the two housings of the output shaft. The results of the blue check test are shown in Figure 2.

a) 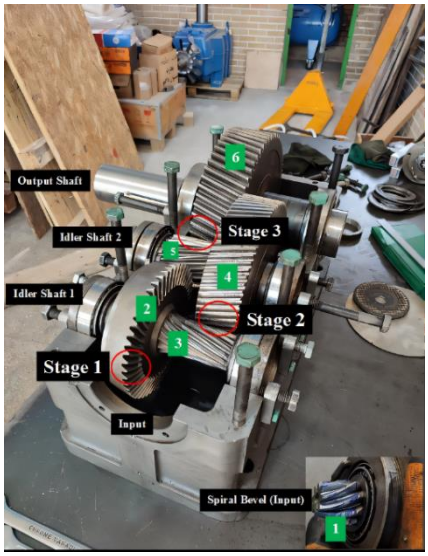

b) 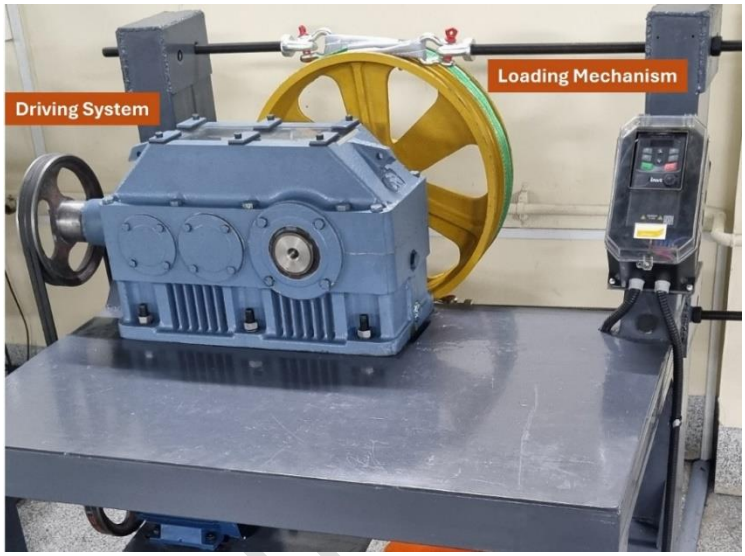

Fig. 1. Experimental test rig: a) Gearbox setup gears, b) Assembled test rig in the laboratory

a) 
b) 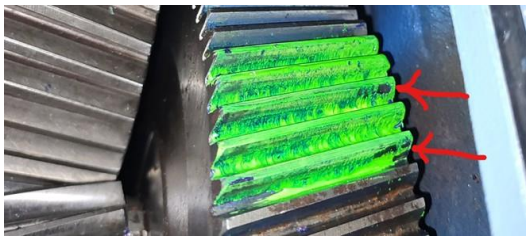

Fig. 2. Blue check test between output and second idler shaft gears: a) Before engagement, b) After engagement

To rectify this defect in the housing, among the available methods, a metal spraying welding technique was employed. This method is highly effective for restoring and correcting the dimensions of mechanical components to their standard condition. In this process, the surface of the defective area is first machined (known as undercutting) to prepare a suitable substrate for the welding alloy. Subsequently, the alloy is sprayed onto the prepared area, and finally, the welded region is re-machined to restore the part to its original standard dimensions. Photographs of the undercutting and welding stages of this procedure, performed on the gearbox used in this study, are presented in Figure 3. Following the corrections and the metal spraying process, the blue check test was repeated, and the concentricity of the output shaft housings was re-evaluated using a dial indicator. The results confirmed that the two housings are correctly aligned.

Accepted Manuscript

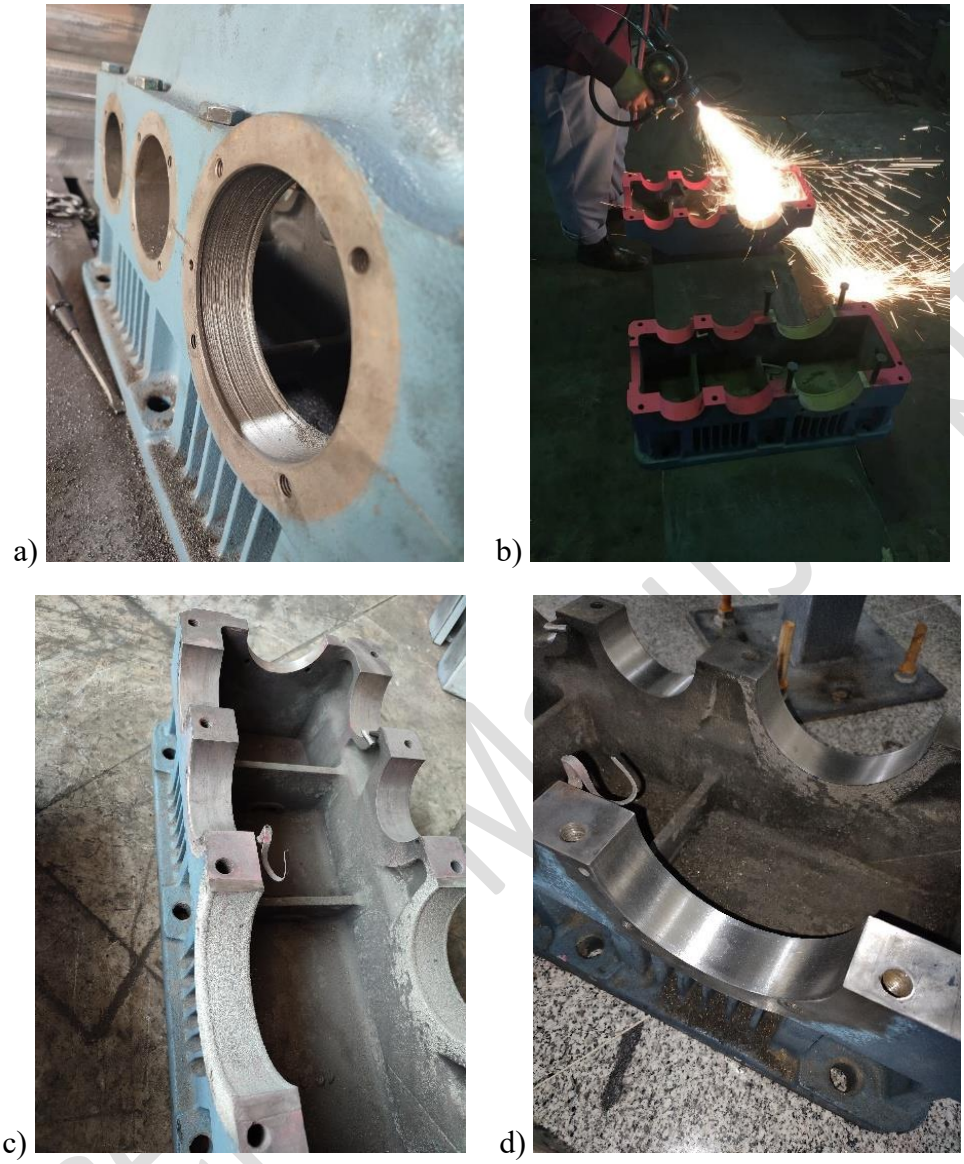

Fig. 3. Metal spray welding process: a) Undercutting, b) Metal spraying, c) Welded area, d) Final area (after final machining)

2.2. Implementation of misalignment between gears

To account for the effects of low operating speeds in misalignment detection for shafts operating under such conditions—and since the output shaft of the current setup operates at 8.5 rpm—misalignments in this study are applied to the output shaft in various planes. Additionally, because the load is applied to the output shaft, this shaft is more prone to becoming misaligned compared to the others. Therefore, introducing misalignment between the output shaft gear and the second idler shaft is of greater importance and significance. After making the necessary corrections to the

gearbox setup, the next step was to search for available bearings from bearing catalogs, such as those from SKF and Timken. The goal is to identify a bearing with the same inner diameter as the one currently on the output shaft, but with a smaller outer diameter. Subsequently, create sufficient clearance between the housing bore and the bearing's outer diameter, allowing the assembly of the mechanism designed to generate misalignment.

The original bearing on the output shaft had an outer diameter of 130 mm and an inner diameter of 90 mm. According to the catalogs, a bearing with the same inner diameter of 90 mm but a smaller outer diameter of 105 mm is available. Considering this selected bearing, the radial clearance between the housing and the bearing is calculated to be 12.5 mm. It should be noted that reducing the outer diameter also decreases the bearing's dynamic and static load capacities. However, given the required service life of the gearbox setup and the experimental objectives, this reduction in load capacity is acceptable. After determining the available clearance for generating misalignment—essentially the eccentricity between the center of the housing bore and the output shaft—the required mechanism was designed.

To induce misalignment, a special end cover was used on the drive-end (DE) of the output shaft. This end cover has two separate parts: an inner part and an outer part. The outer part has an external diameter equal to that of the housing (130 mm) and an internal diameter of 117 mm. Each part has an offset of 1.25 mm, making its geometric center eccentric relative to the center of the DE housing. By rotating these two covers relative to each other, different eccentricities from 0 to 2.5 mm can be achieved in horizontal, vertical, or inclined planes.

The maximum eccentricity occurs when the two covers are assembled so that their eccentricity vectors are aligned in the same direction. Conversely, when the inner and outer covers are assembled with their eccentricity vectors pointing in opposite directions, the output shaft becomes parallel to the second Idler shaft (aligned condition). It should also be noted that during data collection under different operating conditions, the non-drive end (NDE) of the output shaft remained concentric with the shaft and served as the reference point. Figure 4 shows a schematic of the output shaft and the second idler shaft in the aligned condition, designed in SolidWorks. The manufactured end covers used to induce misalignment are shown in Figure 5.

3. Simulations and stress analysis

This section presents simulations conducted in KISSsoft to examine the impact of gear misalignment on tooth stresses. It details the modeling of the output shaft and second idler shaft gears under both aligned and misaligned conditions. Using the contact analysis module, maximum stresses are calculated and compared across different misalignment scenarios. This analysis offers insights into how misalignment affects stress concentration on the gear teeth.

Accepted Manuscript

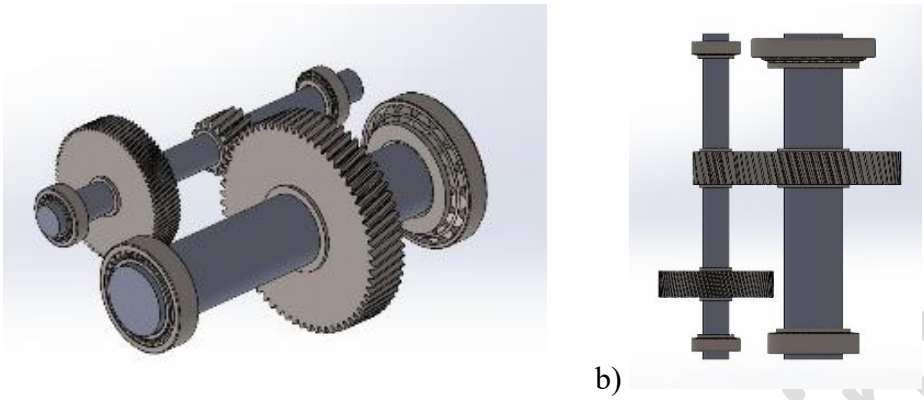

a) b)

Fig. 4. Aligned positions of the output shaft and second idler shaft: a) Isometric view, b) Top view

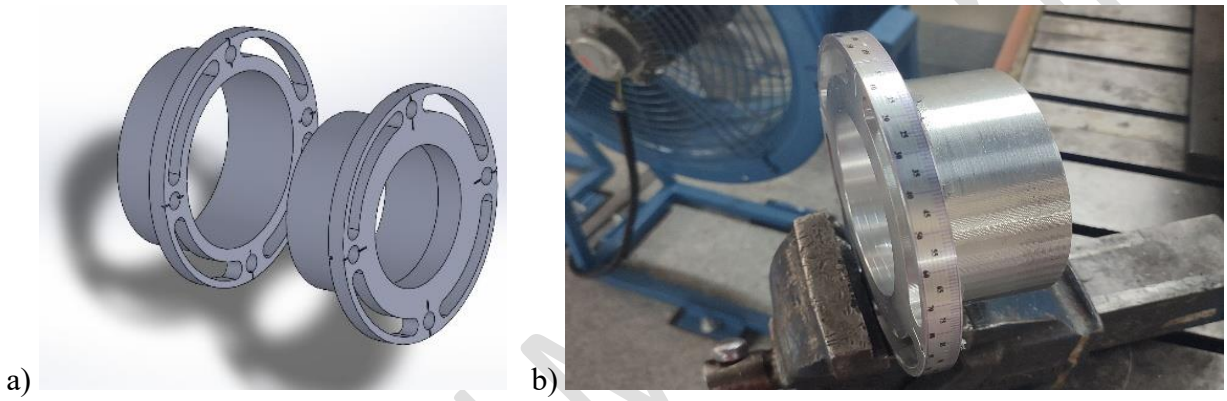

a) b)

Fig. 5. Eccentric end covers: a) SolidWorks model, b) constructed

3.1. Misaligned gear pairs simulated in Kisssoft

In continuation, to investigate the variation of gear-tooth stresses under misalignment introduced by the proposed mechanism, the output shaft and second idler shaft gears were simulated using KISSsoft software. The inner part of the mechanism, as described in Section 2.2, was designed to allow rotation, generating different types and degrees of misalignment at various positions and angles. Accordingly, nine different misalignment scenarios were simulated, including horizontal and vertical misalignments individually, as well as inclined-plane misalignments. Figure 6. a. illustrates the modeled gear pair in the software, while Figure 6. b. shows the gear axes in one of the combined misalignment scenarios (inclined-plane misalignment).

3.2. Misaligned gear pairs stress analysis

Using the contact analysis module of KISSsoft software, the maximum stress values for the two meshing gears were calculated under both misaligned and aligned conditions. To better illustrate the stress increase associated with different misalignment cases, all the obtained results are presented as a histogram. Figure 9 displays the maximum stress values under various conditions.

Accepted Manuscript

As observed, the highest stresses occur when misalignment is introduced in the positive horizontal and vertical directions, resulting in a 4.2% increase compared to the aligned condition.

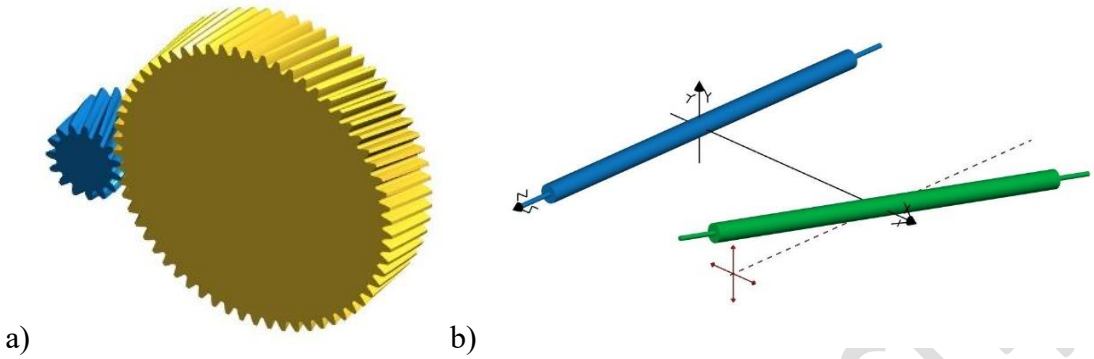

a) b)

Fig. 6. Output and second idler shaft: a) gears, b) misaligned axes simulated in KISSsoft

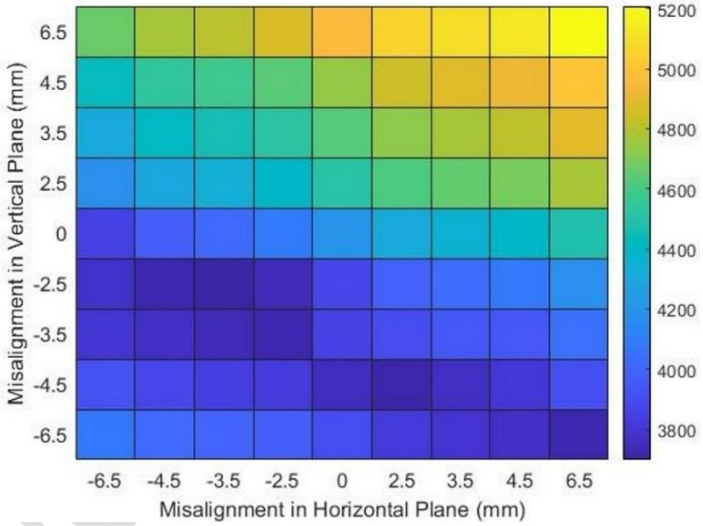

Fig. 7. Hertzian stress (MPa) between the output and the second idler shaft under various misalignment conditions.

4. Signal Processing and Feature Extraction Method

TSA is a widely used technique in condition monitoring and fault diagnosis of gears and power transmission systems. Its primary goal is to remove out-of-phase components and random noise while amplifying components that are phase-synchronized with the shaft rotation or gear meshing. In this process, the vibration signal is resampled based on the shaft's angular speed. By aligning and averaging multiple revolutions, the in-phase components are retained while the others are diminished. The result of this process is the TSA signal, which contains the key vibration pattern caused by gear meshing, along with reduced noise, backlash, and unwanted disturbances. As a

result, considering the advantages of the TSA method and, on the other hand, the industrial nature of the current setup—comprising multiple stages, various bearings, and the presence of noise and uncertainties in the acquired signals—feature extraction based on this method was prioritised. From the extracted TSA signal, several derivative signals are created to enable more accurate fault detection. These include the regular signal, which contains the periodic components related to the gear mesh frequency and its harmonics; the difference signal, which highlights sidebands and impulses caused by localized defects; and the residual signal, which results from removing the regular mesh and shaft-speed components, thereby emphasizing irregular shocks and vibrations associated with faults. Various statistical indicators derived from these signals are then used for gearbox condition monitoring, as shown in Table 2. The parameters x_i, d_i, and r_i represent the i-th sample of the TSA signal, the i-th sample of the difference signal, and the i-th sample of the residual signal, respectively.

Table 2. Features extracted from TSA signals

Feature	**Formula**	**Extracted from (Signal)**
RMS	$\sqrt{\frac{1}{N}\sum_{i=1}^{N} x_i^2}$	TSA
Crest Factor	$\frac{Peak}{RMS}$	TSA
Kurtosis	$\frac{\frac{1}{N}\sum_{i=1}^{N}(x_i - \mu)^4}{\sigma^4}$	TSA
FM4	$\frac{\frac{1}{N}\sum(d_i - \bar{d})^4}{(\frac{1}{N}\sum(d_i - \bar{d})^2)^2}$	Difference
M6A	$\frac{\frac{1}{N}\sum(d_i - \bar{d})^6}{\sigma_d^6}$	Difference
M8A	$\frac{\frac{1}{N}\sum(d_i - \bar{d})^8}{\sigma_d^8}$	Difference
FM0	$\frac{Peak_{TSA}}{RMS_{Reg}}$	Mix
Energy Ratio	$\frac{\sum d_i^2}{\sum R_i^2}$	Difference and Regular
NA4	$\frac{\frac{1}{N}\sum {r_i}^4}{(\overline{\sigma}_r^2)^4}$	Residual

Accepted Manuscript

5. Design of Experiments and Data Acquisition

This section outlines the experimental design and data collection methodology. It begins with an overview of the devices used for vibration measurement and the sensor placement strategy. The loading condition and input speed are then detailed, along with the nine defined misalignment scenarios, which cover both aligned and misaligned conditions. These elements work together to create a systematic and repeatable framework for assessing the sensitivity of features under various operating conditions.

5.1. Data Acquisition Devices and Measurement Points

In this study, vibration data were collected using an STD 3300 dual-channel vibration analyzer. The device's Long Wave module was utilized, with a sampling duration of 90 seconds. In some studies, to extract components related to different frequencies, bands of captured frequencies are often divided into two: low-frequency (5 to 1000 Hz) and high-frequency (1000 to 8000 Hz). However, due to the limitations of the Long Wave module in the STD 3300 device, specifically in setting the lowest frequency to be captured, by the user, separate analysis of low- and high-frequency bands was not performed in this study, and a frequency range of 5–8000 Hz was used to record components across multiple frequencies. Signal extraction was performed using Vibro Designer software. Figure 8 shows the STD 3300 data acquisition system and the connected accelerometer sensor.

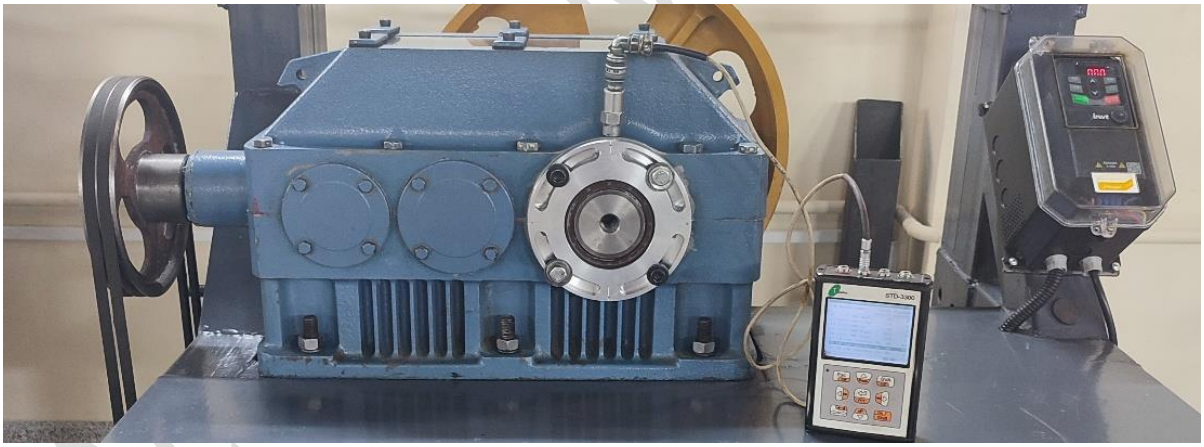

Fig. 8. Data acquisition system

The measurement points are outlined as follows. For the input crown wheel gear, due to limited space and the impossibility of installing sensors on both the drive end (DE) and non-drive end (NDE), vibration signals are recorded from only one side in the horizontal, vertical, and axial directions. For the first idler shaft, second idler shaft, and output shaft, vibration data are collected at both the DE and NDE sides in the vertical, horizontal, and axial directions, except at the NDE side's axial direction, where no sensor is installed. The measurement locations are shown in Figure 9.

Accepted Manuscript

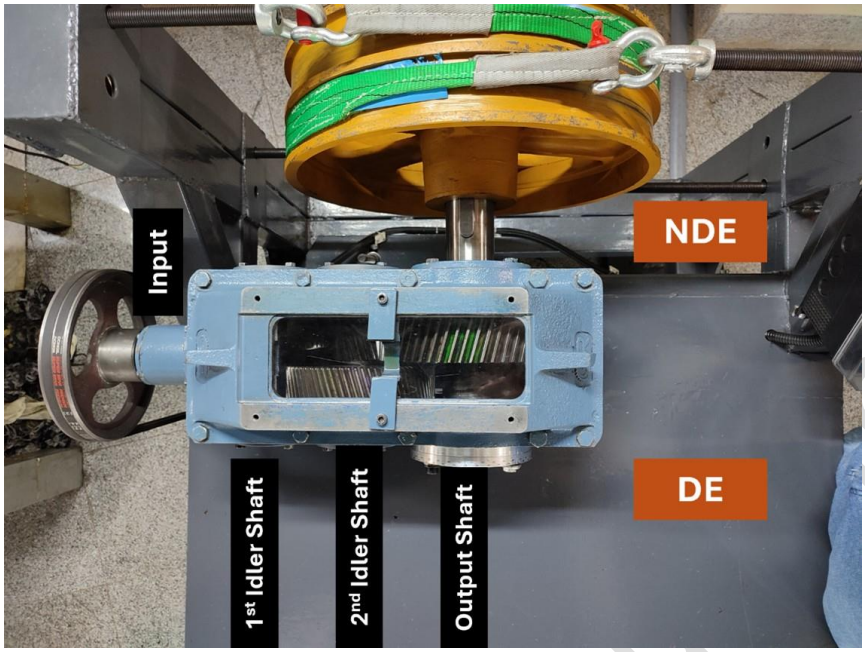

Fig. 9. Measurement points

5.2. Loading, Speed, and Misalignment Scenarios

During data acquisition, the gearbox is subjected to high loading. To apply this loading, all four screws of the belt-driven loading mechanism were uniformly tightened to a specific magnitude and specific length of bolts. This magnitude value was recorded as the reference for maximum loading and was subsequently used to apply a consistent maximum load during the tests. Additionally, the input speed is adjusted to the maximum nominal motor speed of 25 Hz. For a comprehensive analysis of various misalignment conditions and their comparison with the aligned condition, a total of eight misalignment levels were defined. Together with the aligned condition, nine scenarios were identified, for which the values of the considered features were examined. To achieve the maximum misalignment in different planes, from the magnitude aspect, the eccentricity vectors of the end covers were aligned together in all scenarios, resulting in an eccentricity of 2.5 mm. The criterion for defining the considered levels is the rotation angle of the eccentricity vector of the end covers. To better illustrate each misalignment level examined during data acquisition, SolidWorks simulations are performed for the corresponding conditions. Furthermore, to enhance the understanding of each misalignment condition and to clearly indicate the angle and magnitude of the applied misalignment, angular markings were also added to the SolidWorks-generated illustrations. For instance, for the first misalignment level, the eccentricity vector is oriented along the positive horizontal axis, which is hereafter referred to as the 0° level (Figure 10). In the second level, the eccentricity vector formed a 45° angle with the positive horizontal axis, denoted as the 45° level (Figure 11). The same approach was applied to the other

Accepted Manuscript

levels, where the orientation of the eccentricity vector determines the naming convention. Table 3 summarizes all misalignment levels investigated in this study.

Table 3. Levels of misalignment in this study

Misalignment angle (degree)	0	45	90	135	180	225	270	315
Misalignment plane	Horizontal	Inclined	Vertical	Inclined	Horizontal	Inclined	Vertical	Inclined
Naming in this study	0 deg	45 deg	90 deg	135 deg	180 deg	225 deg	270 deg	315 deg

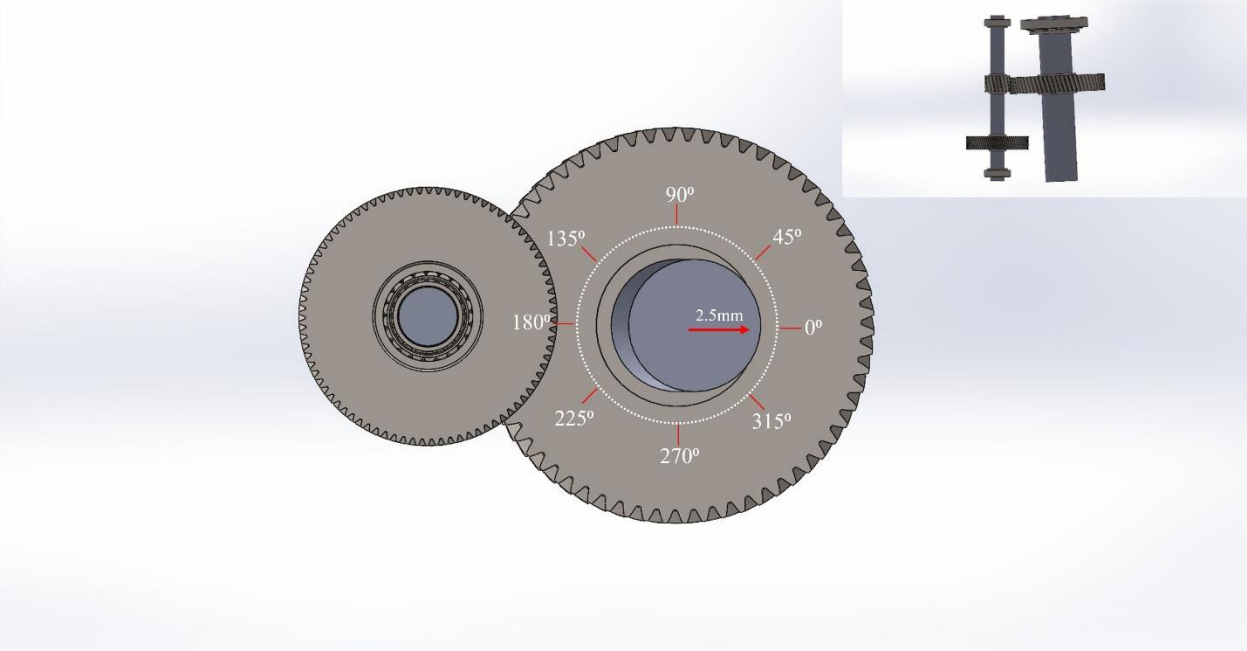

Fig. 10. Front and top views of misalignment in the horizontal plane (0 degrees) in SolidWorks

Manuscript

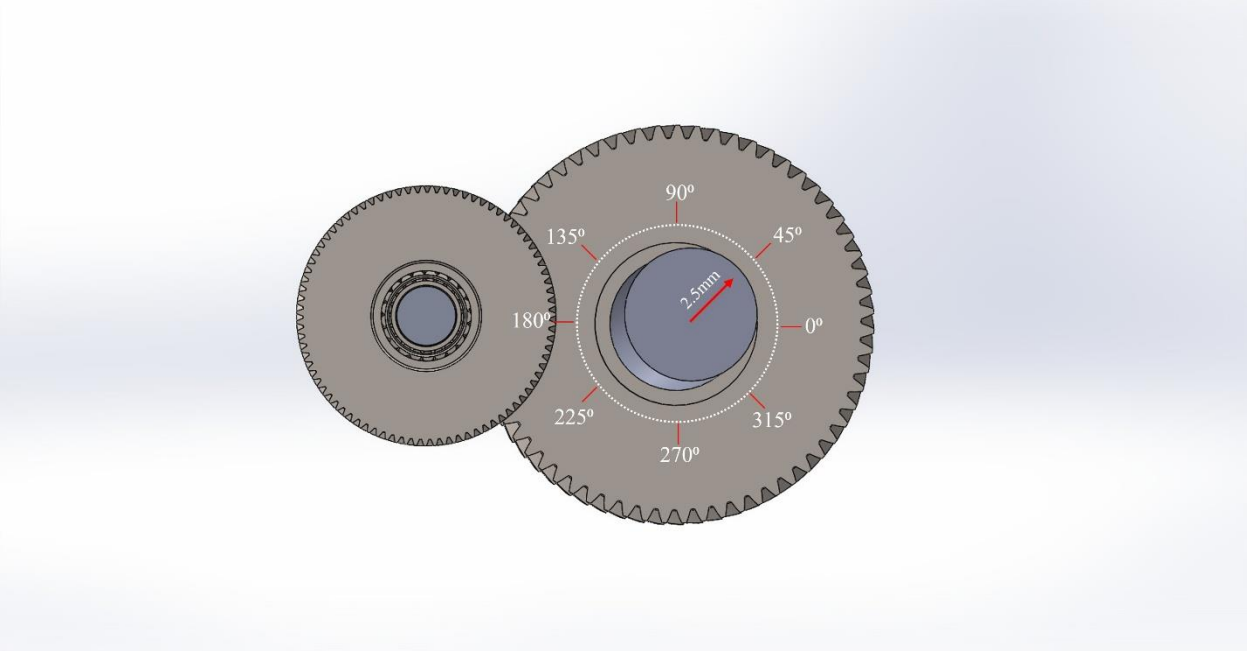

Fig. 11. Front view of misalignment on the inclined plane (45 degrees) in SolidWorks

6. Results and Discussion

In this section, diagrams are presented to illustrate the variation trends of each feature under different misalignment and aligned conditions. The horizontal axis of these diagrams represents the eight misalignment levels along with one aligned level, while the vertical axis indicates the value of the corresponding feature for a specific direction and frequency range. In each diagram, the variation of the feature is displayed simultaneously for all gearbox shafts (sensor locations), allowing for direct comparison. Moreover, each diagram corresponds to a particular feature in different measurement directions (horizontal, vertical, and axial) and is plotted separately for both velocity and acceleration parameters. As mentioned in Section 5, all data were acquired at the maximum speed (25 Hz, the nominal motor speed) under the maximum applied load, with a frequency range of 5–8000 Hz. For example, Figures 13 and 14 illustrate the variation of the Energy Ratio feature for both velocity and acceleration signals.

Accepted Manu

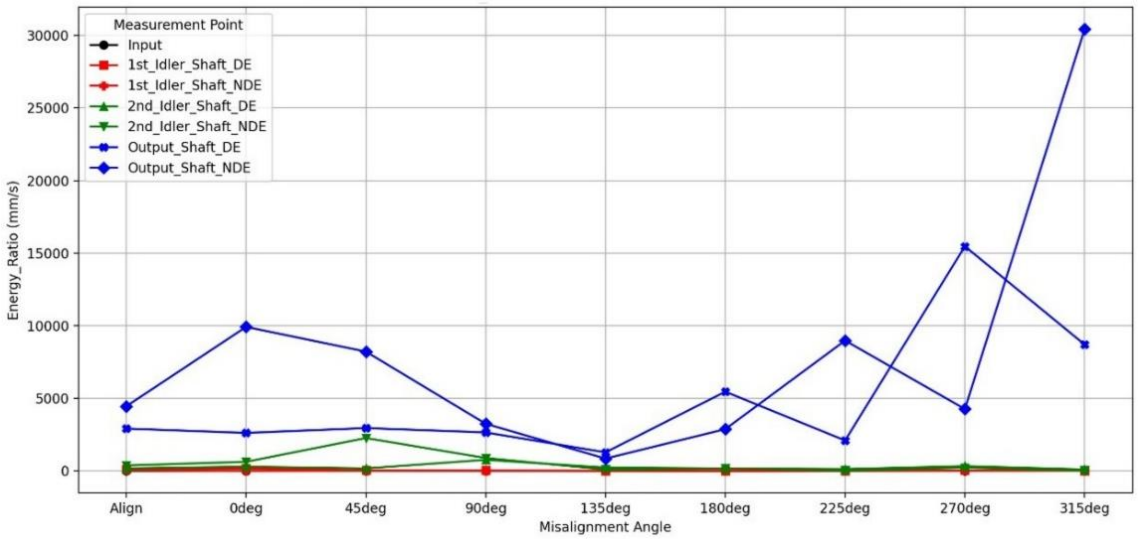

Fig. 13. Variation of the energy ratio feature across different misalignment angles for the velocity signal.

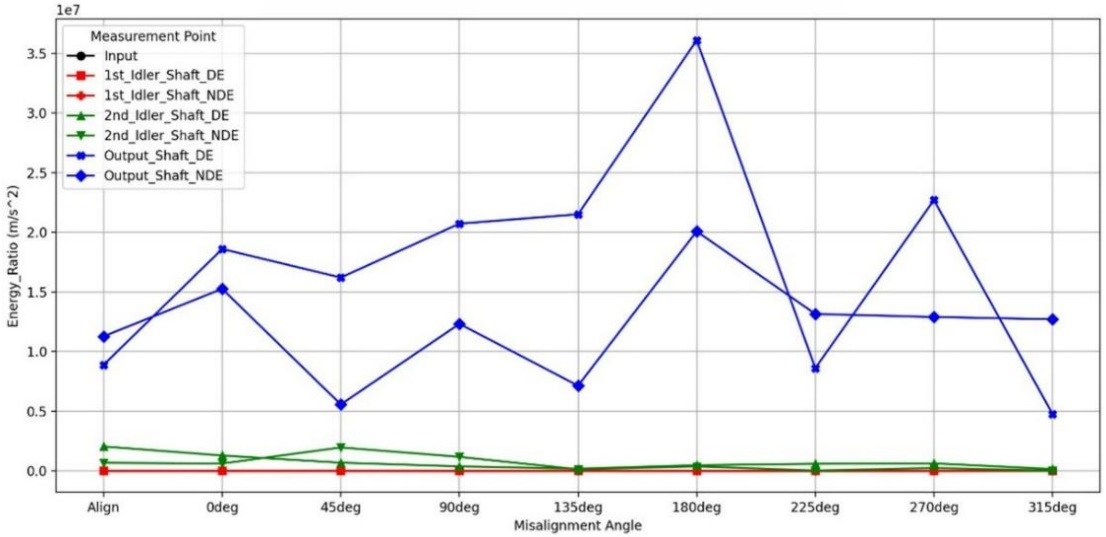

Fig. 14. Variation of the energy ratio feature at different misalignment angles for the acceleration signal

In this study, the relationship between stress values at different misalignment levels was also examined using the stress contours from Section 3. It was observed that changes in misalignment do not cause a consistent overall increase or decrease in tooth stress. Specifically, the variation of stress values across different misalignment cases was not symmetrical (Figure 15).

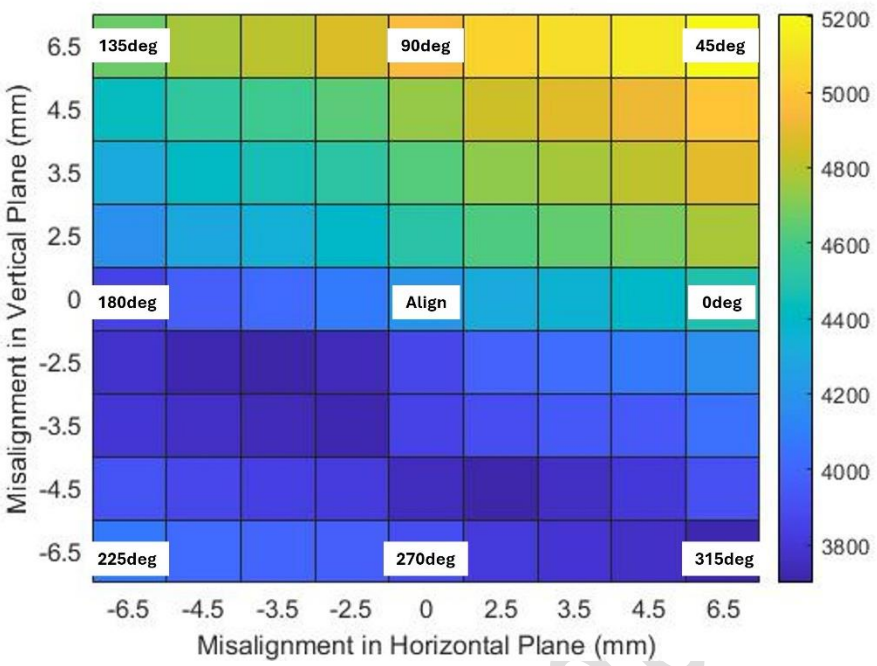

Fig. 15. Scenarios of misalignment and Hertzian stress values

For further analysis of features, to evaluate their sensitivity regarding the aligned condition, a series of boxplots is generated. For each measurement point, the absolute percentage variation of each feature relative to the aligned condition was calculated using the following equation:

$$\Delta = \left| \frac{Misaligned\ magnitude - Aligned\ magnitude}{Aligned\ magnitude} \right| \times 100 \qquad (1)$$

For each combination of DE or NDE side–velocity or acceleration signal–measurement direction, a boxplot was created, where the horizontal axis shows the features, and the vertical axis displays the percentage variation from the aligned condition. Above each box, the feature value in the aligned condition (Align) is noted to emphasize the effect of the reference magnitude on the calculated percentage variation. This method allows for quick, visual comparisons of the features, making it easier to identify those most sensitive to changes in the misalignment angle. For instance, Figures 16 and 17 show two boxplots: one for the DE side in the horizontal direction and another for the NDE side in the vertical direction, both related to the output shaft and based on the acceleration signal.

Accepted Manuscript

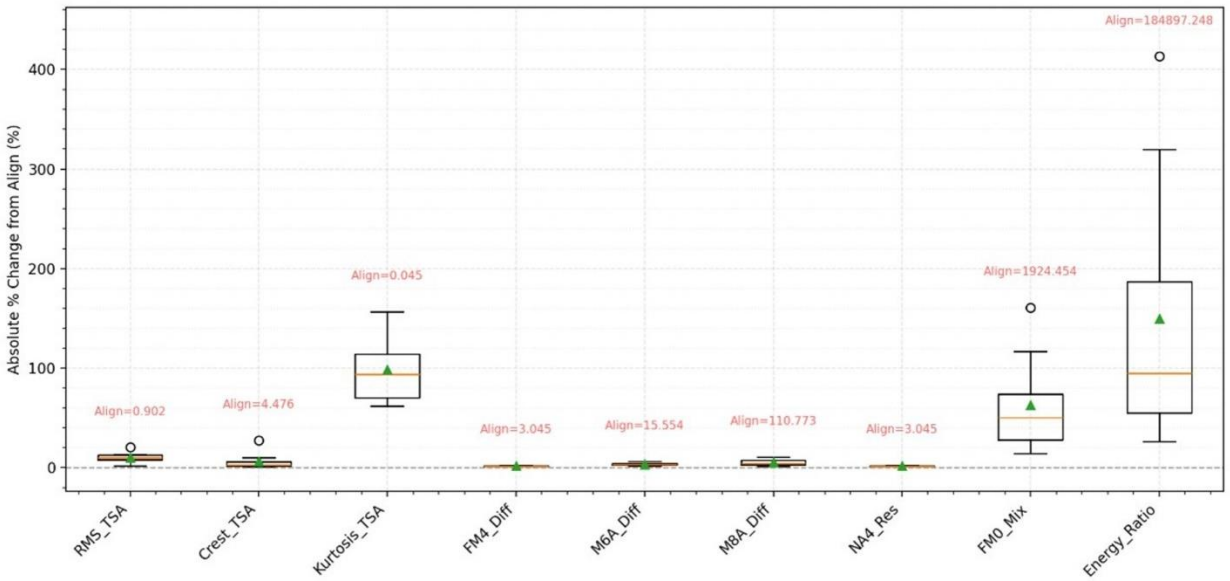

Fig. 16. Variation in the alignment state of the output shaft DE within the velocity signal in the horizontal direction.

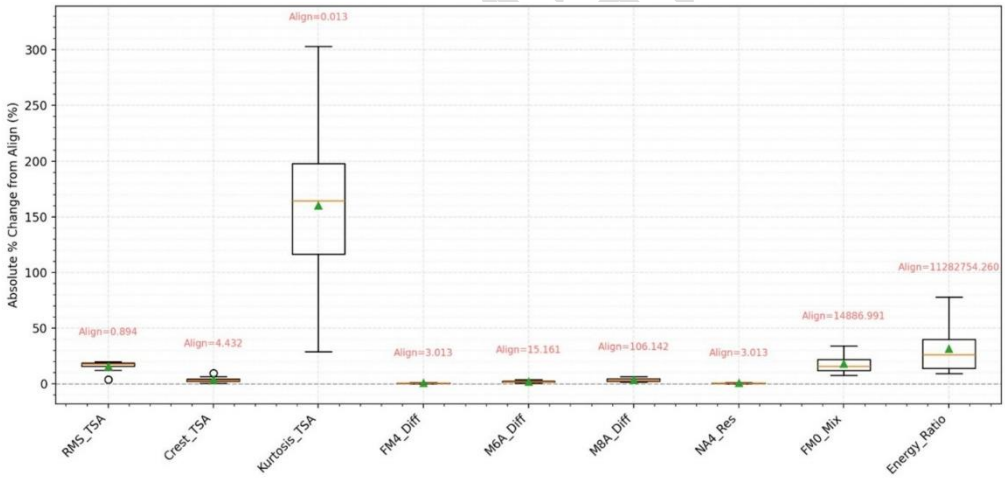

Fig. 17. Variation in the alignment state of the output shaft NDE in the acceleration signal along the vertical direction

To identify the most suitable features for misalignment detection, this study evaluated features based on their maximum percentage variation relative to the aligned condition. In the boxplots, the feature with the most significant deviation from the reference line (the horizontal axis) indicates the highest percentage change compared to the aligned state. Additionally, features with shorter box lengths along the vertical axis show lower sensitivity to variations in the misalignment plane, with their changes primarily depending on the magnitude of misalignment. Table 4 lists the features exhibiting the highest variations relative to the aligned condition across all measurement points. As shown in Table 4, Kurtosis and Energy Ratio demonstrated the most significant

variations in this dataset. To further examine the behavior of the extracted features concerning misalignment, additional analyses were performed on the collected data. The focus here is on two features—Kurtosis and Energy Ratio—that showed the most prominent variations. Data from all measurement points, including the input shaft, the first and second idler shafts, and the output shaft on both DE and NDE sides, were analyzed separately in three measurement directions: horizontal, vertical, and axial. Furthermore, both acceleration and velocity vibration signals were analyzed independently.

Table 4. Features with the most significant variations compared to the aligned condition across all measurement points

	Horizontal		Vertical		Axial
	DE	NDE	DE	NDE	DE
	Velocity (mm/s)				
Input	Energy Ratio		M8A		Energy Ratio
1st Idler Shaft	Kurtosis	Kurtosis	Kurtosis	M8A	Kurtosis
2nd Idler Shaft	Energy Ratio	Kurtosis	Kurtosis	Kurtosis	M8A
Output Shaft	Energy Ratio	Energy Ratio	Kurtosis	Kurtosis	Energy Ratio
	Acceleration (m/s^2)				
Input	Energy Ratio		Kurtosis		Kurtosis
1st Idler Shaft	Kurtosis	Kurtosis	Kurtosis	Energy Ratio	Energy Ratio
2nd Idler Shaft	Kurtosis	Energy Ratio	Kurtosis	Kurtosis	Kurtosis
Output Shaft	Energy Ratio	Kurtosis	Kurtosis	Kurtosis	Kurtosis

The analysis procedure is as follows: for each measurement point, direction, and signal type, the maximum variation was calculated and displayed in the form of bar charts. These plots enabled a direct comparison of the sensitivity of each measurement point to misalignment. To provide a more comprehensive perspective, the results across all measurement points were also aggregated into heatmaps. In these heatmaps, the horizontal axis represents the measurement direction, the vertical axis corresponds to the measurement points (shafts and sides), and the color scale denotes the maximum variation of the selected feature. This visualization facilitated the rapid identification of locations and directions most sensitive to misalignment. According to the bar chart results (Fig. 18), it was observed that Kurtosis and Energy Ratio exhibited the highest relative variations at the NDE side of the second idler shaft and at both DE and NDE sides of the output shaft.

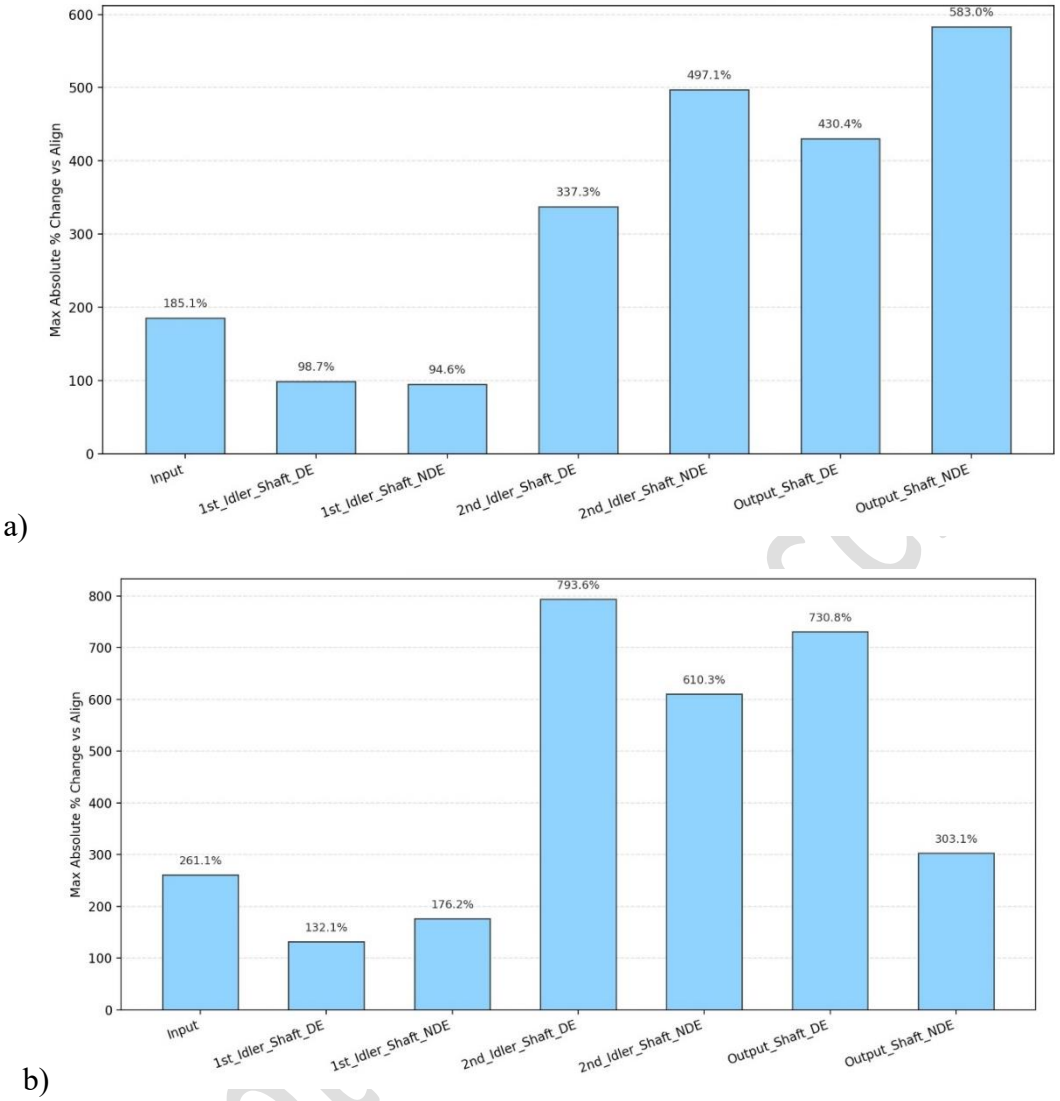

Fig. 18. Maximum variation of selected features at different measurement points: a) Energy ratio, velocity signal, in the vertical direction, b) Kurtosis, acceleration signal

Furthermore, a comparison of the three measurement directions revealed that horizontal measurements exhibited the most significant variations at these locations, underscoring their high sensitivity to misalignment. This is clearly supported by the heatmap representations (Fig. 19). From a signal-domain perspective, comparing velocity- and acceleration-based results showed that both signals exhibited similar trends, with the selected features showing the most significant variations at the output shaft and the second idler shaft (especially on the NDE side). This indicates that the sensitivity of these features to misalignment is not strongly affected by the type of signal. Overall, the findings reveal that the closer the measurement point is to where misalignment occurs (i.e., the NDE side of the output shaft and the second idler shaft), the greater the variation in the features compared to the aligned reference condition.

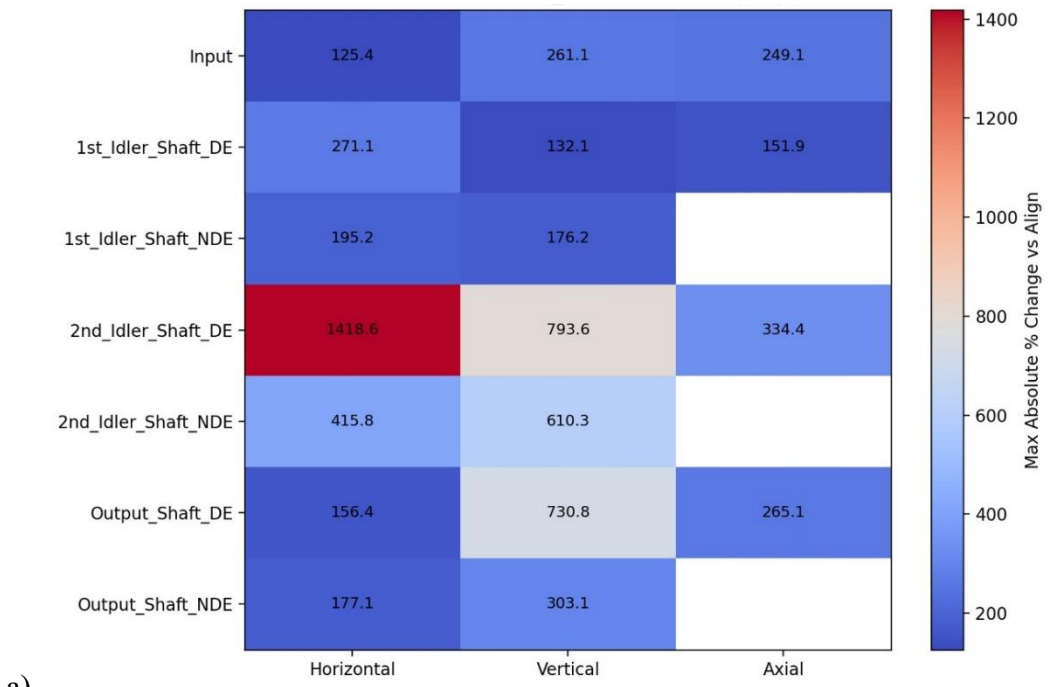

a)

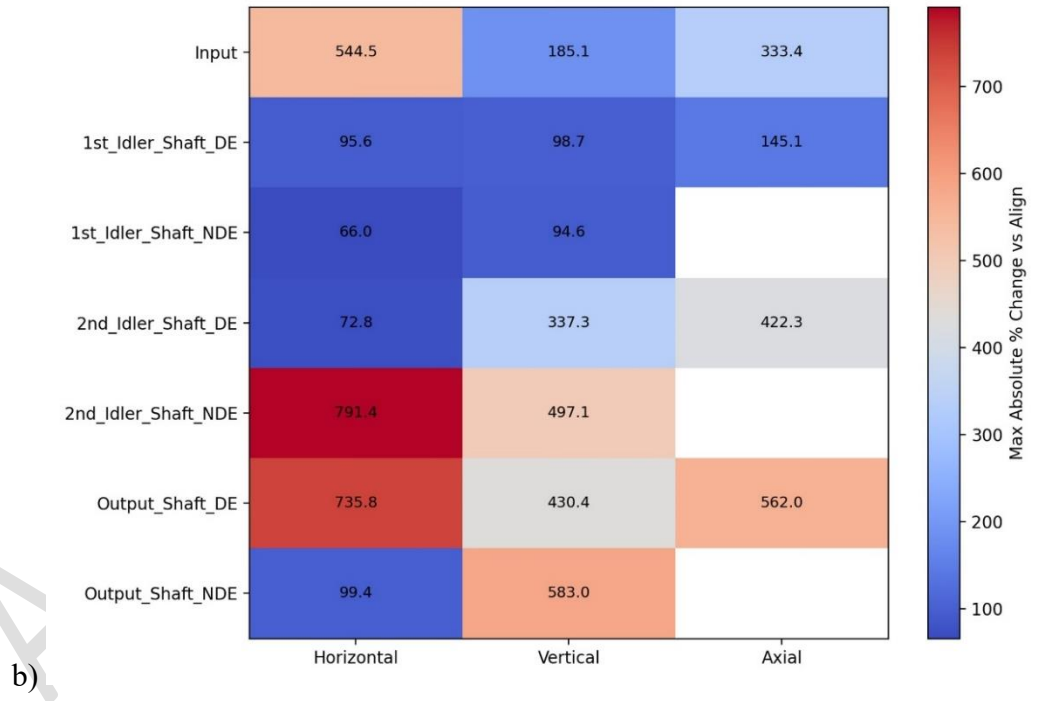

b)

Fig. 19. Maximum variation of selected features at different measurement points and directions: a) Energy ratio, velocity signal; b) Kurtosis, acceleration signal.

7. Summary/ Conclusion

In this study, an industrial gearbox test rig was used, and a mechanism was designed and built to simulate gear misalignment in its output shaft. Due to its ability to rotate at different angles, this mechanism could replicate various types of misalignments in different planes. The engagement of the two gears under different misalignment conditions was analyzed using KISSsoft software, and the maximum stresses were identified. Results showed that misalignments in inclined planes—especially in the first quadrant of the hypothetical circle (i.e., misalignment along the positive horizontal and vertical axes)—caused the highest stress concentration and increase. This can be attributed to the gear helix angle and the direction of forces on the teeth. The study found that Kurtosis and Energy Ratio are the most sensitive features among those examined, showing the greatest variation compared to the aligned condition. These features can be effectively used to detect gear misalignment. Both Kurtosis and Energy Ratio increased more significantly when misalignment was present, with their maximum changes occurring at the output shaft (both DE and NDE sides) and on the NDE side of the second idler shaft. Furthermore, these variations were more pronounced in the horizontal direction compared to other directions, and this pattern was consistent across velocity and acceleration signals. Therefore, the proximity of the measurement point to the misaligned stage significantly influences feature sensitivity. In future studies, these features could be utilized to develop intelligent models, thereby accelerating the fault diagnosis process for industrial gearboxes. Moreover, the application of methods such as wavelet energy spectrum analysis, spectral kurtosis, and time–frequency domain analysis is deemed essential for future studies on fault diagnosis in this type of industrial setup.

Acknowledgements

The authors would like to sincerely thank Behravesh Vibration Engineering Company, the Machine Tools Workshop at Sharif University of Technology, the Technical Manager of Hamsoo Company, Eng. Amirhossein Hosseini, Ali Janmohammadi, and everyone who supported us in this research.

Accepted Manuscript

References

[1] G. He, K. Ding, W. Li, and X. Jiao, "A novel order tracking method for wind turbine planetary gearbox vibration analysis based on discrete spectrum correction technique," *Renewable Energy,* vol. 87, pp. 364-375, 2016.

[2] M. A. Khan *et al.*, "Gear misalignment diagnosis using statistical features of vibration and airborne sound spectrums," *Measurement,* vol. 145, pp. 419-435, 2019.

[3] P. Kane and A. Andhare, "Critical evaluation and comparison of psychoacoustics, acoustics, and vibration features for gear fault correlation and classification," *Measurement,* vol. 154, p. 107495, 2020.

[4] E. Caso, A. Fernandez-del-Rincon, P. Garcia, M. Iglesias, and F. Viadero, "Monitoring of misalignment in low-speed geared shafts with acoustic emission sensors," *Applied Acoustics,* vol. 159, p. 107092, 2020.

[5] L. Yang *et al.*, "Dynamic characteristic analysis of spur gear system considering tooth contact state caused by shaft misalignment," *Nonlinear Dynamics,* vol. 109, no. 3, pp. 1591-1615, 2022.

[6] V. Prasad SR, J. Poulose, and A. Sadique, "Fault Detection of Spur Gear Using Machine Learning," in *Proceedings of the International Conference on Aerospace & Mechanical Engineering (ICAME 21)*, 2022.

[7] Y.-H. Hu, Q.-G. Du, and S.-H. Xie, "Nonlinear dynamic modeling and analysis of spur gears considering uncertain interval shaft misalignment with multiple degrees of freedom," *Mechanical Systems and Signal Processing,* vol. 193, p. 110261, 2023.

[8] D. Zou, L. Wang, L. Yang, W. Yu, and L. Xie, "Dynamic characteristics of a spur gear pair under the coupled effects of angular misalignment fault and tooth modification," *International Journal of Non-Linear Mechanics,* vol. 155, p. 104453, 2023.

[9] W.-q. Zhao, J. Liu, W.-h. Zhao, H. Wang, and N. Yang, "Modeling and vibration feature analysis of a spur gear-bearing system with a misaligned shaft angle," *Nonlinear Dynamics,* vol. 112, no. 1, pp. 151-174, 2024.

Accepted Manuscript